HHS Public Access

Author manuscript

*Mol Cancer Res*. Author manuscript; available in PMC 2022 November 04.

Published in final edited form as:

*Mol Cancer Res*. 2022 August 05; 20(8): 1208–1221. doi:10.1158/1541-7786.MCR-21-0888.

# MUC16 Promotes Liver Metastasis of Pancreatic Ductal Adenocarcinoma by Upregulating NRP2-Associated Cell Adhesion

**Saravanakumar Marimuthu**[1], **Imayavaramban Lakshmanan**[1], **Sakthivel Muniyan**[1], **Shailendra K. Gautam**[1], **Rama Krishna Nimmakayala**[1], **Sanchita Rauth**[1], **Pranita Atri**[1], **Ashu Shah**[1], **Namita Bhyravbhatla**[1], **Kavita Mallya**[1], **Paul M. Grandgenett**[2], **Michael A. Hollingsworth**[2], **Kaustubh Datta**[1,2], **Maneesh Jain**[1,2], **Moorthy P. Ponnusamy**[1,2,3,*], **Surinder K. Batra**[1,2,3,*]

[1]Department of Biochemistry and Molecular Biology, College of Medicine, University of Nebraska Medical Center, Omaha, NE, USA.

[2]Eppley Institute for Research in Cancer and Allied Diseases, Fred & Pamela Buffett Cancer Center, University of Nebraska Medical Center, Omaha, NE, USA.

[3]Department of Pathology and Microbiology, College of Medicine, University of Nebraska Medical Center, Omaha, NE, USA.

## Abstract

Pancreatic ductal adenocarcinoma (PDAC) is one of the most lethal types of cancer, as it commonly metastasizes to the liver resulting in an overall poor prognosis. However, the molecular mechanism involved in liver metastasis remains poorly understood. Here, we aimed to identify the MUC16-mediated molecular mechanism of PDAC-liver metastasis. Previous studies demonstrated that MUC16 and its C-terminal (Cter) domain are involved in the aggressiveness of PDAC. In the present study, we observed MUC16 and its Cter expression significantly high in human PDAC tissues, PDAC organoids, and metastatic liver tissues, while no expression was observed in normal pancreatic tissues using immunohistochemistry (IHC) and immunofluorescence (IFC) analyses. MUC16 knockdown in SW1990 and CD18/HPAF PDAC cells significantly decreased the colony formation, migration, and endothelial/p-selectin binding. In contrast, MUC16-Cter ectopic overexpression showed significantly increased colony formation and motility in MiaPaCa2

[*]Correspondence: Surinder K. Batra, Ph. D. and Moorthy P Ponnusamy, Ph.D. Department of Biochemistry and Molecular Biology, University of Nebraska Medical Center, Omaha, Nebraska, 68198-5870, USA. Phone: 402-559-1170, Fax: 402-559-6650, sbatra@unmc.edu (S.K.B) or mpalanim@unmc.edu.

Authors contributions

SKM, MPP, and SKB conceived and designed the experiments. SKM, IL, SM, RKN, SR PA, AS, NB, KM, performed the experiments. PMG and MAH provided the rapid autopsy primary and metastatic samples. SKG, IL, SM, SR, RKN, PA, AS, NB, KM assisted with in vitro and in vivo experiments. SKM, IL, SM, SR, RKN, PA, AS, NB, KM, KD, and MJ analyzed the data. SKM, MPP, SKB, and MJ wrote and edited the manuscript. All authors have read and approved the final manuscript.

**Conflict of interest:** SKB and MAH are the co-founders of Sanguine Diagnostics and Therapeutics, Inc. The other authors declare no potential conflicts of interest.

Ethics approval and consent to participate

Not applicable

Consent for publication

Not applicable

PC cells. Interestingly, MUC16 promoted cell survival and colonization in the liver, mimicking an ex vivo environment. Furthermore, MUC16 enhanced liver metastasis in the *in vivo* mouse model. Our integrated analyses of RNA-seq suggested that MUC16 alters Neuropilin-2 (NRP2) and cell adhesion molecules in PC cells. Furthermore, we identified that MUC16 regulated NRP2 via JAK2/STAT1 signaling in PDAC. NRP2 knockdown in MUC16 overexpressed PDAC cells showed significantly decreased cell adhesion and migration. Overall, the findings indicate that MUC16 regulates NRP2 and induces metastasis in PDAC.

**Implications:** This study shows that MUC16 plays a critical role in PDAC liver metastasis by mediating NRP2 regulation by JAK2/STAT1 axis, thereby paving the way for future therapy efforts for metastatic PDAC.

## Graphical Abstract

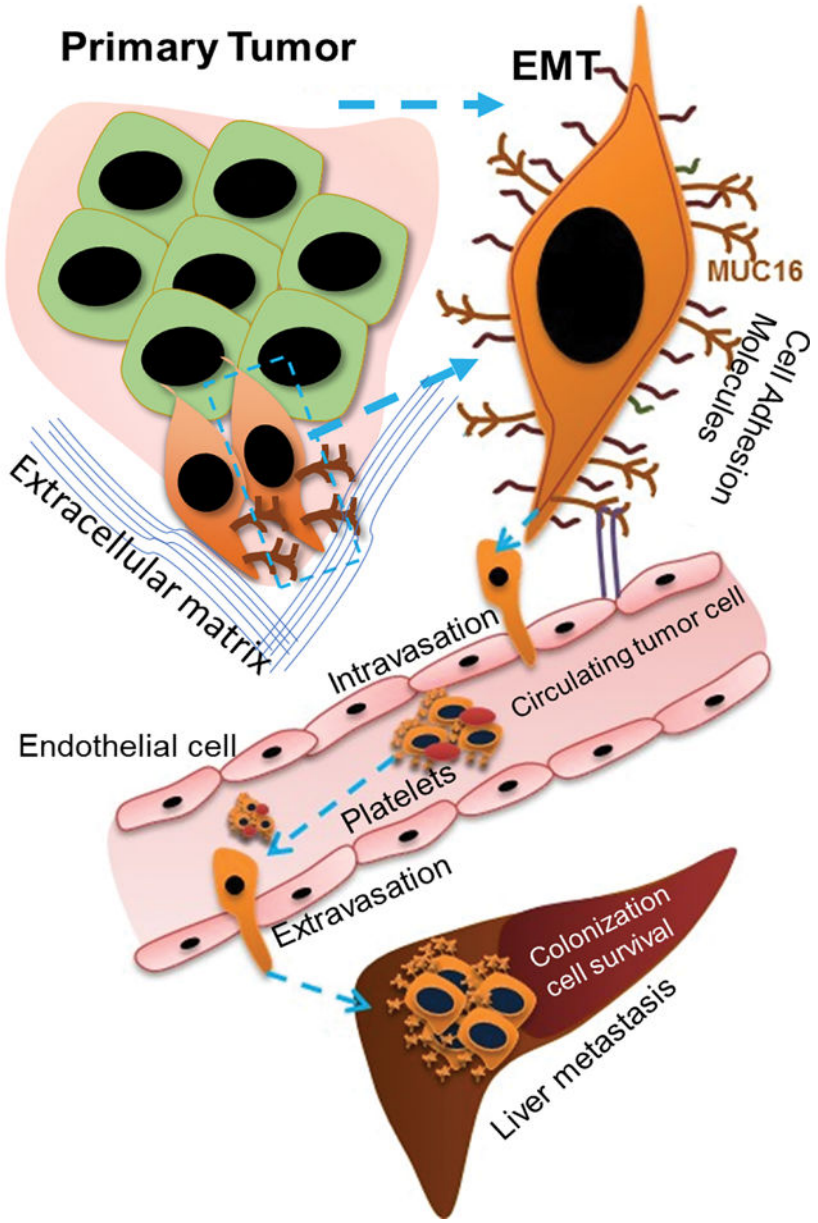


**Keywords**

MUC16; PDAC organoids; Neuropilin-2; Cell adhesion molecules; Liver metastasis

## Introduction

Pancreatic cancer is the third leading cause of cancer deaths in the United States, with an overall five-year survival rate that ranges from 5% to 15% (1,2). The poor survival is attributed to 'its' aggressive metastatic nature, making PDAC one of the most lethal cancers. PDAC frequently metastasizes to the liver in over half of patients (3,4), partially due to the

hepatic portal circulation. However, the underlying molecular mechanism that drives PDAC cells towards the liver is poorly understood.

MUC16 is a type-I transmembrane heavily glycosylated protein comprised of extracellular N-terminal domain, tandem repeat domain, and a C-terminal (Cter) domain (5–7). MUC16 (also known as CA125) is the gold standard biomarker used to diagnose and monitor disease progression and recurrence in ovarian cancer (8). The overexpression of MUC16 is seen in pancreatic (6), ovarian (9), cervical (10), breast (11), lung (12), and esophageal (13) cancers. An earlier study from our lab has proved that MUC16 is expressed in primary and metastatic pancreatic cancer (PC) tumors, thus implying that MUC16 has a vital role in the progression and metastasis of PDAC (6). The knockdown of MUC16 leads to enhanced expression of epithelial markers and reduced expression of mesenchymal markers in cells. Moreover, the loss of MUC16 demonstrated decreased FAK-mediated Akt and ERK/MAPK activation and pancreatic cancer tumor growth and metastasis (7). Elevated levels of MUC16 in the circulation and expression are generally linked with poor prognosis in PDAC (14).

Our previous study demonstrated that the cleavage of MUC16 occurs in the Golgi/post-Golgi compartments, and the cleaved MUC16 translocates to the nucleus and is involved in the regulation of LMO2 and NANOG expression (15,16). We also observed that the MUC16 carboxyl-terminal (Cter) transfected PC cells displayed increased proliferation, motility, and upregulation of stemness-specific genes (16).

Neuropilins (NRPs) are type-I transmembrane glycoproteins with cytoplasmic domains to transduce biological signals (17). NRPs are of two types, NRP1 and NRP2. The overexpression of NRP2 has been observed in various types of cancer; it has often been associated with poor prognosis in PDAC (18–20), colorectal carcinomas (21), osteosarcoma (22), prostate cancer (23), and breast cancer (24). NRP2 expressed in cancer cells facilitates vascular adhesion and extravasation by interacting with α5 integrin on endothelial cells ((25).

However, the organ tropism, potential functions, and MUC16 mediated molecular mechanisms via which NRP-2 promotes PDAC metastasis are still unclear. This study shows that MUC16 and MUC16-Cter are progressively expressed in PDAC and liver metastatic tissues. Our *in vitro* results demonstrate that MUC16 and its cleavage regulate cell adhesion properties and induce the liver metastatic potential of PDAC cells using *in vivo* models.

## Materials and methods

### Cell lines

MiaPaCa-2 (Cat# ATCC® CRL-1420), human umbilical vein endothelial cell (HUVEC) (Cat# ATCC® PCS-100–010), SW1990 (Cat# ATCC® CRL-2172), human microvascular endothelium (HMEC-1) (Cat# ATCC® CRL-3243), cells were purchased from American Type Culture Collection (ATCC, Manassas, VA). Human immortalized hepatocytes, Fa2N4 (Cat# IFH15), MFE support medium, and MFE plating medium were purchased from XenoTech LLC (Lenexa, KS). Human hepatic stellate cell LX-2 was a gift from Professor Scott L. Friedman, MD, Icahn School of Medicine at Mount Sinai, NY, USA. MiaPaCa-2,

T3M4 (RRID:CVCL_4056), Capan1, CD18/HPAF, SW1990 cells were grown adherently in Dulbecco's Modified Eagle's Medium (DMEM) high glucose, supplemented with 10% fetal bovine serum (FBS) and 1% penicillin-streptomycin. HMEC-1 (RRID:CVCL_0307) cells were grown in MCDB131 medium supplemented with 10 ng/mL epidermal growth factor (EGF), 1 μg/mL Hydrocortisone, 10mM Glutamine and 10 % FBS. The HUVEC cells were grown in vascular cell basal medium (ATCC® PCS-100–030) supplemented with endothelial cell growth kit-BBE (ATCC® PCS-100–040), and penicillin-streptomycin. The LX-2 (RRID:CVCL_5792) cells were cultured in DMEM high glucose and supplemented with 2% FBS and 1% penicillin-streptomycin. For 3D *in vitro* culture and sphere culture, cells were cultured in a stem cell medium containing DMEM/F12 medium supplemented with 1% B27, 20 ng/mL, EGF, and 10ng/mL basic fibroblast growth factor (bFGF). All the cell lines were cultured at 37 °C with 5% $CO_2$ in a humidified atmosphere. For the doxycycline-inducible shRNA expressing stable cells were treated with doxycycline 1 μg/mL for 48hrs. All the cells were tested for mycoplasma free and authenticated by short tandem repeat (STR) profiling.

## Human PDAC primary tissue organoid culture

Human PDAC tumors were used to generate 3D organoids, as discussed previously (26). We have developed organoids from PDAC (n=8) and adjacent normal (n=5) tissues. Briefly, PDAC tissues were digested using Collagenase II and dispersed, and the digested tissue was mixed with matrigel. Droplets of ~20 μL were plated in a 48-well culture plate (Cat# M9312, Greiner CELLSTAR, Sigma, USA). After 10–15 minutes, a pre-warmed organoid medium was added to the plate and cultured for six days. Organoids from normal pancreatic tissue remain normal in organoid culture for 4 to 5 passages. The organoid medium is supplemented with human recombinant Wnt3a (Cat#5036-WNP-010/CF, R&D Systems), human recombinant R-Spondin1 (Cat # 4645-RS-100/CF, R&D Systems), B27 supplement (Cat# 17504–044, Life Technologies), 1,25 mM N-acetyl-l-cysteine (Cat# A9165, Sigma-Aldrich)10 mM nicotinamide (Cat# N0636, Sigma-Aldrich), 50 ng/mL human EGF (Cat# AF-100–15, PeproTech), 500 nM A83–01, 100 ng/mL human recombinant FGF10 (Cat# 100–26, PeproTech), 10 nM gastrin (Cat# 3006, R&D Systems), and Noggin (Cat# 6057-NG-100/CF, R&D Systems).

## Gene silencing by siRNAs, shRNAs, and inhibitors

For stable cell lines, doxycycline-inducible MUC16 shRNA stable cell lines (SW1990 and CD18/HPAF cells) were developed using human MUC16 shRNA (Cat# RHS4696–200693582, Dharmacon, Illinois, USA) TRIPZ Inducible Lentiviral shRNA plasmid according to the ' 'manufacturer's instructions. MUC16 gene knockout by CRISPR/Cas9 based MUC16 KO in the Capan1 cell line was developed as described in our previous study (7). CMV9-F114AA plasmid was used for MUC16-Cter overexpression in MiaPaCa2 and T3M4 cells, and construct details were described (16). Transient KD of STAT1 siRNA (Cat # sc-44123, Santa Cruz Biotechnology, USA) and NRP2 (Cat# SR305825, OriGene, Rockville MD, USA) were used for silencing STAT1 and NRP2 expression in Capan1 and SW1990 PC cells. Post transfection of 36 hrs or 48 hrs transient knockdown of NRP2 cells used for experiments. The Capan1 and SW1990 cells were treated with JAK2 inhibitor

(Fedratinib – Cat# S2736, Selleckchem) and STAT1 inhibitor (Fludarabine, Cat# S1491, Selleckchem) at 6μM or 10μM respectively at 48hrs.

### Tumor cell -endothelial and -p-selectin binding assay

Tumor-endothelial cells adhesion assay (Cat# CBA215, Cell Biolabs, Inc.) was performed to study the cell-cell interaction. 96 well plate was pre-coated with 0.1% gelatin, and HMEC-1 endothelial cells were grown as a monolayer in 96 well plate. For activation, HMEC-1 cells were treated with TNFα (10 ng/mL) for 12 h. Tumor cells (Capan1 MU16 KO, SW1990 MUC16 KD, CD18/HPAF MUC16 KD, transient knockdown of NRP2 in Capan1, SW1990 cells vs. control cells) were grown as a monolayer and prepared a cell suspension at $1\times10^6$ cells/mL in serum-free (SF) medium and added fluorescent dye (CytoTracker) and incubated for 1 h in $CO_2$ at 37 °C for 60 min, then gently washed with SF medium. The pre-labeled tumor cells were resuspended, and $0.2\times10^6$ cells/mL was added into activated endothelial cells and incubated in 5% $CO_2$ at 37 °C for 90 min. Then cells were gently washed with wash buffer (3x, 5 min) to remove the unbinding tumor cells. For p-selectin binding assay, the protocol by Li et al. (27) was followed with modifications, 96 well plate was pre-coated with human recombinant p-selectin/CD62P protein (Cat#ADP3, R&D system) (10 μg/mL) for 12 h at 4°C, after that the wells were washed with PBS and blocked with 1% BSA for 1h. After blocking and washing, pre-labeled tumor $0.2\times10^6$ cells/well were added into p-selectin pre-coated 96 well plates and incubated in 5% $CO_2$ at 37 °C for 90 min. Then cells were gently washed with PBS (3x, 5 min) to remove the unbinding tumor cells. Representative images were taken under a fluorescence microscope (EVOS FL Auto Imaging System- Thermo Fisher Scientific), following which the cells were lysed with cells lysis buffer for 5 min at RT. Then 96 well-read with a fluorescence plate reader (Multi-mode reader, Synerge Neo2, BioTeK, VT, USA) or (SpectraMax M3, Molecular Devices, CA, USA) at 480/520nm.

### *In vitro* human liver metastasis model: 3 D culture and sphere formation assay

Human normal liver tissue samples were obtained from RAP at UNMC. The human liver metastasis model *in vitro* 3D culture and liver decellularization method is briefly described in our previous study (28). In order to develop *in vitro* PDAC metastasis model, doxycycline-inducible MUC16 shRNA expressing SW1990 cells were tagged with GFP and treated with or without doxycycline for 48 h. SW1990 MUC16 KD $GFP^+$ cells were mixed with human endothelial cells (HUVEC), human hepatic stellate cells (LX-2), human hepatocytes (Fa2N4), and human liver decellularized scaffold. The cell mix was prepared at a density of $1X\ 10^5$ cells/ml, and 500 μg/ml of the decellularized liver scaffold was mixed and seeded into 96 well ultra-low attachment plate in DMEM F12 supplemented with β-FGF (3 ng/mL), EGF (3 ng/mL), VEGF (2 ng/mL), 1% B27 supplement, and 1% penicillin-streptomycin incubated in 5% $CO_2$ at 37 °C for 24 h. Then the plate was transferred to Incucyte for 12 days (Incucyte® S3 Live-Cell Analysis System). The green fluorescence protein was measured, images were taken, and video clips were recorded by the automated system every 3 h and bright field and corresponding green fluorescence images were taken under a fluorescence microscope (EVOS FL Auto Imaging System- Thermo Fisher Scientific). We used SW1990 MUC16 KD GFP+ cells grown as a monolayer with or without doxycycline treatment for the spheroid formation study. 15,000 cells/well were

seeded into 96 well ultra-low attachment plate with stem cell medium (DMEM-F12 with supplements) incubated in 5% $CO_2$ at 37 °C for 24 hrs, and then the plate was transferred to Incucyte for 8 days. Clonogenic cell growth images and video were recorded as per the method mentioned above. All the samples were triplicated and analyzed in Incucyte® SX5 Analysis Software.

### *In vivo* PDAC metastasis model by hemi-spleen injection technique

All animal experiments were performed in compliance with procedures approved by the Institutional Animal Care and Use Committee at the University of Nebraska Medical Center (UNMC). As described previously, the hemi-spleen technique was used to generate the liver metastasis model (29,30). The mice were anesthetized, and left subcostal incision was made to expose the spleen. The spleen was cut into two parts from the middle of two medium-sized hemoclips to avoid splenic bleeding and leakage. The distal end was then pushed back into the abdominal cavity to prevent contamination, and the proximal part of the spleen was used for injection. The mice (age 8–10 weeks) were randomized into two groups, the Capan1 control, and Capan1 MUC16 KO cells were tagged with firefly luciferase (Cat# LP464–100, GeneCopoeia). A stock of $1\times10^7$ cells/ml in PBS was prepared. 50 µl cells were taken in 150µl PBS prefilled syringe, and the syringe was kept vertical so that the interface between cells and PBS was maintained. The bevel was dipped in 70% ethanol, and cells were slowly injected with a follow-up flushing of PBS. Once flushed, medium and small size hemoclips were applied to the distal end of the pancreas and splenic vein to avoid the backflow of the injected cells. The hemi-spleen was removed, and after the saline flush, the sutures and wound clips were applied to seal the peritoneal cavity, and mice were kept for recovery as per the IACUC guideline. After 2 weeks of injection, we performed luminescence imaging using IVIS available at the animal core facility.

### Statistical analysis

All data are presented as the mean ± SD samples (n=3). Statistical significance was analysed using Student t-test (*p<0.05, **p<0.01, ***p<0.001). Microsoft Excel (RRID:SCR_016137) and GraphPad Prism (RRID:SCR_002798) (version 9.0) were used for statistical analysis.

## Results

### Expression of MUC16 and MUC16-Cter in human primary pancreatic cancer, liver, and lung metastasis tissues

We analyzed MUC16 expression profiles in the human primary pancreatic tumor, liver-metastasis, and lung-metastasis samples using the GSE71729 data set. PDAC liver metastasis samples showed significantly higher MUC16 expression compared to the primary tumor (Figure 1 A), and no significant difference was observed between primary vs. PDAC lung metastatic samples. Immunohistochemistry (IHC) analysis showed MUC16 staining in the apical membrane whereas MUC16-Cter stained cytoplasmic and nuclear region of the primary tumor (Figure 1 B), and PDAC liver metastasis (Figure 1 C) and lung-metastasis tumor samples (Supplementary Figure 1 A, B). H-score showed that MUC16 and MUC16-Cter expression is higher in the primary PC tumor and liver-metastasis (Figure 1 D, E). In

addition, we stained MUC16 and Cytokeratin 19 (CK19) in patient-derived PDAC tumor organoids and normal pancreas organoids from the normal adjutant area. Interestingly, our results show that MUC16 and MUC16-Cter are overexpressed in PDAC tumors, and no expression was observed in normal pancreatic ductal organoids. PDAC organoids showed larger size with MUC16 expression compared to normal organoids (Figure 1 F, G). CK19, a marker of ductal adenocarcinomas and proliferation expressed in both normal and PDAC derived tumors. These results strongly suggest that MUC16 and MUC16-Cter overexpressed in PDAC and liver metastatic samples.

## Loss of MUC16 reduces *in-vitro* tumorigenic and migratory potential in PC cells

Immunoblot analysis confirmed the MUC16 expression in CRISPR/Cas9-based MUC16 gene knockout (KO) Capan1 cells and doxycycline-induced MUC16-shRNA expression (MUC16 knockdown (KD) in SW1990 and CD18/HPAF cell lines (Figure 2 A, B, C). Immunofluorescence analysis also showed decreased MUC16 expression in MUC16 KD in SW1990 and CD18/HPAF cells (Supplementary Figure 2 A, B). In addition, MUC16 non-expressing (MiaPaCa2) and MUC16 expressing (T3M4) PC cells were stably transfected with carboxyl-terminal MUC16. The overexpression was confirmed in MiaPaCa2 and T3M4 cells (Figure 2 D).

To explore the tumorigenic and metastatic potential of MUC16, *in vitro* tumorigenic and migratory assays were performed. MUC16 silenced PC cells (Capan1, SW1990, and CD18/HPAF) showed significantly (*** $p<0.001$, *$p<0.05$) decreased colony-forming ability compared to respective control cells (Figure 2 E, F, Supplementary Figure 2 C). Whereas MUC16-Cter overexpressed cells showed significantly (**$p<0.01$) increased clonogenic survival compared to vector (CMV9) control transfected MiaPaCa2 cells (Figure 2 G). Further, we tested the migratory potential of MUC16 KD PC cells using a trans-well migration chamber assay. Our results showed a decreased migratory potential of Capan1 MUC16 KO and SW1990 MUC16 KD cells, while the number of migratory cells is significantly (**$p<0.01$, *** $p<0.001$) increased in MUC16-Cter overexpressed cells (Figure 2 H, I, J). These results suggest that MUC16 and MUC16-Cter play a role *in vitro* clonogenic and migratory potential of PC cells.

## MUC16 promotes cell-cell interaction during the metastatic spread of PDAC

We further analyzed the role of MUC16 in tumor cell - nontumor cell interaction during the metastatic spread of PC cells. Endothelial cell binding assay showed a significantly (***$p<0.001$, **$p<0.01$) reduced endothelial cell binding capability in Capan1 MUC16 KO, SW1990 MUC16 KD, and CD18/HPAF MUC16 KD cells compared to control cells (Figure 2 K, L, M, Supplementary Figure 2 D). Furthermore, we examined the interaction of MUC16 expressing tumor cells with p-selectin (platelets) during metastatic spread. The p-selectin binding assay showed significantly (***$p<0.001$, **$p<0.01$) decreased p-selectin binding on Capan1 MUC16 KO, SW1990 MUC16 KD, and CD18/HPAF MUC16 KD cells compared to MUC16 expressing PC control cells (Figure 2 N, O, P, Supplementary Figure 2 E). These results suggest that MUC16 could facilitate PC cell interaction with endothelial cells and p-selectin during the metastatic spread of PC cells.

## The potential role of MUC16 in pancreatic tumor cell survival in liver-specific metastatic *ex vivo* environments

Based on our observation that MUC16 is significantly overexpressed in liver metastasis compared to primary as well as lung metastatic tumor tissues, we investigated whether MUC16 expressing PC cells could colonize and survive *ex vivo* liver-specific metastatic model (28,31) (Figure 3 A). For this, we tagged SW1990 MUC16 KD cells with a green fluorescent protein (SW1990 $GFP^+$ cells) and seeded them with human endothelial cells (HUVEC), human hepatic stellate cells (LX-2), and human hepatocytes (Fa2N4) cells in ultra-low attachment plates. The cells were cultured for 10 days, and half of the media were changed with/without doxycycline every two days. The $GFP^+$ cell growth was monitored continuously every three hours by an automated Incucyte live cell imaging system. Our results showed after 8 days that the survival and colonization of MUC16 expressing cells drastically increased in liver mimicking *ex vivo* environment compared to the dox treated MUC16 KD cells (Figure 3 B, C, D, Supplementary Video 1, 2). These results strongly suggest that MUC16 plays a role during PC cell colonization and survival in liver metastasis. We also studied the tumor sphere-forming ability of MUC16 expressing (SW1990) tumor cells using these ultra-low attachment plates. Our data shows that MUC16 expressing cells grow aggressively in an anchorage-independent environment compared to MUC16 KD PC cells. Representative images of $GFP^+$ spheroids and their corresponding bright-field images and growth curves generated from the Incucyte are shown in Figures 3 E, 3 F, 3 G, Supplementary Video 3, 4). Our findings cumulatively suggest that MUC16 promotes *in vitro* colonization and cell survival in a metastatic liver environment.

## Identification of cell adhesion molecules and metastasis genes expression in MUC16 Knockout and MUC16-Cter overexpressed PC cells

We have done global RNA-Seq analysis from MUC16 Knockout Capan1 and MUC16-Cter overexpressed MiaPaCa2 PC cells. Further, we classified into downregulated or upregulated genes from KO and overexpressed cells. Based on RNA-Seq log2 (fold change) values, we have shown the top 50 altered genes as a heat-map under MUC16 knockout and MUC16-Cter overexpressed conditions. We validated the top 25 downregulated genes from Capan1 MUC16 KO and the top 25 upregulated genes from MiaPaCa2 MUC16-Cter overexpressed cell line by QRT-PCR analysis (Figure 4 A, Supplementary Figure 3 A, B). To determine the common genes among MUC16 KO and MUC16-Cter overexpressed conditions, we intersected the top differentially expressed genes. Interestingly, a comparison of the top 50 genes from each of those groups showed 10 genes that are common in both groups, i.e., IGFBP3, COL6A3, FSTL1, SERPINE1, MMP1, TGFBI, NRP2, BDNF, SDC1, and MSX1 (Figure 4 B). Cell adhesion molecules have a vital role in metastasis and progression of cancer. The cell-cell interactions between tumor cells and the endothelium, platelets, and leukocytes promote metastasis and contribute to tumor cell adhesion, extravasation, and the establishment of metastatic lesions (32). Subsequently, we studied whether MUC16 has a role in the regulation of cell adhesion gene expression in PC cells. Based on log2 values from our RNA-seq analysis, we observed alteration of MUC16 mediated cell adhesion genes CDH1, CDH2, CDH3, CDH6, CDH10, CDH12, CDH23, CDH24, PCDHA1, PCDHB12, PCDH8, PCDH9, DSG1, DSG2, DSG3, DSG2-AS-1 DSC1, DSC2, and DSC3 in KD and overexpression models (Figure 4 C). Pathway analysis shows that MUC16 plays a potential

role in regulating the cell-cell adhesion mediated by Cadherin and extracellular matrix (ECM) molecules (Figure 4 D). In addition, our enrichment plot data shows that the vascular endothelial growth factor (VEGF) signaling pathways and ECM protein and ATP-binding cassette (ABC) transporters genes are downregulated in MUC16 KO cells (Figure 4 E). Our data analysis using the GSE19279 dataset shows that Desmocollin 3 expression was significantly high in PC metastasis when compared to the normal pancreas (Supplementary Figure 4). These observations strongly prove that MUC16 regulates metastasis promoting genes and cell adhesion molecules in PDAC

## MUC16 promotes cell adhesion genes and metastatic gene NRP2 regulation through activation of JAK2/STAT1 oncogenic pathway

By validating cell adhesion genes, we identified the significant variation of *Cadherin 24, Desmocollin 3, Procadherin B12* gene expression in knockout/knockdown and overexpression models (Figure 5 A). Further, we determined the protein expression by immunoblot and immunofluorescence analysis, and the results indicate that the expression levels of Desmocollin 3 and Procadherin B12 are decreased in Capan1 MUC16 KO PC cells and increased in MUC16-Cter overexpressed MiaPaCa2 cells (Figure 5 B, C). These results strongly suggest that MUC16 has a key role in the regulation of cell adhesion-promoting genes in PDAC.

In addition, we also investigated the MUC16 associated metastatic gene expression. Our QRT-PCR data shows that *PTHLH*, *IGFBP2*, *GADD45A*, *FBLN2*, *PTTG1*, *JUN*, *SERPINE1*, *TGFBI*, and *NRP2* mRNA expression are commonly altered in both MUC16 KO and Cter overexpressed PC cells (Figure 5 D). Further, we detected the copy number of each gene using digital droplet-PCR (ddPCR). ddPCR absolute quantification results show *SERPINE1*, *NRP2*, *IGFBP2*, and *PTTG1* genes copy numbers are significantly decreased in MUC16 KO cells, while those genes are significantly increased in MUC16-Cter overexpressed PC cells (Supplementary Figure 5). Additionally, validation of these genes from the GSE19279 dataset showed that *SERPINE1*, *IGFBP2*, and *NRP2* expression are higher in PDAC and liver-metastasis compared to the normal pancreas (Supplementary Figure 6). Interestingly, we identified the MUC16-mediated metastasis genes such as PAI1 (*SERPINE1*), *IGFBP2*, and *NRP2* in PC cells. Our immunoblot and immunofluorescence analysis show that *NRP2* expression is decreased in MUC16 knockout/knockdown Capan1/SW1990 cells, and *NRP2* is overexpressed in MUC16-Cter overexpressed T3M4 and MiaPaCa2 cells (Figure 5 E, F). However, *IGFBP2* is overexpressed in MUC16-Cter overexpressed T3M4, MiaPaCa2 cells but not altered in MUC16 KO/KD cells. PAI1 is overexpressed in MUC16-Cter overexpressed MiaPaCa2 cells. Nevertheless, the expression of PAI1 in MUC16-Cter overexpressed T3M4 and KD/KO cells are altered (Supplementary Figure 7).

Subsequently, we investigated the molecular mechanism of MUC16 mediated NRP2 regulation in PC cells. Earlier, we showed that MUC16 could interact with JAK kinase to promote MUC16-mediated cell proliferation/survival (11). This study observed that the STAT1 transcription factor is significantly altered in MUC16 overexpression and knockdown conditions. We performed immunoblot analyses to determine the association

between these molecules in PC cells. Our immunoblot results demonstrated that STAT1 phosphorylation decreased in MUC16 knockout Capan1 and knockdown SW1990 cells and upregulated in MUC16-Cter overexpressed MiaPaCa2 and T3M4 cells. JAK2, an upstream signaling pathway for STAT1, showed reduced phosphorylation in MUC16 KD/KO cells and increased in MUC16-Cter overexpressed cells compared to the control cells (Figure 5 E). Subsequently, to determine the relation between MUC16, JAK2 STAT1, and NRP2, we performed inhibition of JAK2 phosphorylation (Y1007/08) using specific inhibitor Fedratinib. Our immunoblot results showed that the inhibition of JAK2 phosphorylation lead to downregulation of STAT1 phosphorylation (Y701) and NRP2 expression in MUC16 expressing Capan1 and SW1990 PC cells (Figure 5 G). These observations strongly suggest that MUC16 regulates NRP2 through the activation of JAK/STAT1 signaling in PC cells, which leads to the induction of metastasis in PDAC.

### Association of MUC16 silencing with altered expression of EMT markers in PDAC

Epithelial to mesenchymal transition (EMT) is an important underlying phenomenon for metastasis; we evaluated the expression of EMT markers in MUC16-Cter expressing MiaPaCa2 and T3M4 cells and MUC16 KO Capan1 cells. MUC16-Cter overexpressed cells correlate with increased N-cadherin, Snail, Vimentin expression (Supplementary Figure 8 A, B). Also, MUC16 knockout Capan1 cells showed decreased expression levels of N-cadherin. While epithelial cell-specific markers such as cytokeratin 18 and E-cadherin markedly increased and/or not altered in MUC16 knockout cells (Supplementary Figure 8 C). Together, these results provide compelling evidence that MUC16 deficiency or proficiency leads to epithelial to mesenchymal transition and therefore contributes to the metastatic behavior of PDAC cells.

### Effect of NRP2 downregulation reduces the *in-vitro* migratory potential, tumor cells-endothelial and p-selectin binding in PC cells

We identified that MUC16 regulates the metastatic promoting gene NRP2 in PC cells.To determine the relation between STAT1 and NRP2, we performed Stat1 knockdown using STAT1 inhibitor or siRNA in MUC16 expressing Capan1 and SW190 cells. Our results showed the inhibition of STAT1 phosphorylation using a specific inhibitor, Fludarabine. The inhibition of STAT1 phosphorylation resulted in decreased NRP2 expression in Capan1 and SW1990 PC cells (Figure 6 A).

In addition, the knockdown of STAT1 using siRNA showed decreased NRP2 expression in both Capan1 and SW1990 PC cells (Figure 6 B). These observations strongly suggest that MUC16 regulates NRP2 through the activation of JAK/STAT1 signaling in PC cells, which leads to the induction of metastasis in PDAC. Next, we determined the functional impact on NRP2 silencing in PC cells. Our Immunoblot analysis confirmed the NRP2 KD in Capan1 and SW1990 cells (Figure 6 C). The knockdown of NRP2 showed significantly (*** $p<0.001$, ** $p<0.01$) decreased migratory potential compared to control cells (Figure 6 D, E). NRP2 KD cells (Capan1 and SW199) were used for endothelial and p- selectin binding study. Our results showed significantly (*** $p<0.001$, ** $p<0.01$) reduced endothelial cell binding in Capan1 NRP2 KD and SW1990 NRP2 KD cells compared to control cells (Figure 6 F, G). The P-selectin binding assay demonstrated significantly (* $p<0.05$,

**p<0.01) decreased p-selectin binding in Capan1 NRP2 KD and SW1990 NRP2 KD cells compared to NRP2 expressing PC control cells (Figure 6 H, I). Our finding strongly suggests that NRP2 promotes PC cell interaction with endothelial cells and selectin during the metastatic cascade of PC cells.

### MUC16 mediates liver metastasis in PDAC in hemi-spleen implantation

To study the role of MUC16 in PDAC liver metastasis, we injected a luciferase tagged Capan1 control and MUC16 KO cell lines using a hemi-spleen orthotopic model in the athymic nude mice. Tumor growth and metastasis were monitored every 10 days using an IVIS imaging system after injecting D-luciferin substrate intraperitoneally (Figure 6 J). After 21 days, the mice injected with control cells developed a primary tumor and metastasis. Mice injected with MUC16 KO cells did not develop liver metastasis compared to controls (Figure 6 K). However, MUC16 KO and control cells showed tumor growth in the pancreas, and no metastasis developed in the lung (Figure 6 K). Correspondingly, the representative histology of the pancreatic tumor, lung, and liver metastasis is shown (Figure 6 L). These results showed the role of MUC16 in PDAC liver metastatic in vivo study. Overall, our finding strongly supports that MUC16 expressing PC cells has a role in EMT, endothelial cell communication, and intravasation. Also, MUC16 helps tumor cells to recolonize and cell survival in secondary organs like the liver. MUC16 promotes cell adhesion molecules and metastasis genes by activating the JAK2/STAT1 oncogenic signaling axis (Figure 6 M).

## Discussion

In pancreatic cancer, ~53% of the patients were diagnosed with an advanced metastatic stage (33). The liver is the most common site for pancreatic cancer metastasis (34,35). Cancer progression and metastasis are promoted by cell adhesion molecules (32). Cell adhesion molecules facilitate the endothelial adhesion of tumor cells, and the tumor cells interact with endothelial through integrins, selectins, and platelets (36). A study has shown that MUC16 is associated with cell adhesion and possibly aids in ovarian cancer metastasis (37). Moreover, MUC16 is linked with E-cadherin and β-catenin, which participate in the regulation of cell adhesion (38).

MUC16 is not expressed in normal pancreatic ducts, but it is over-expressed in PC and is strongly linked to PC metastasis (6,7,16). The previous study demonstrates that the expression of MUC16 increases stage-wise from PanIN I to PanIN III, and it is highly expressed in PDAC (6). Furthermore, we demonstrated the metastatic potential of MUC16 and Cter in PC cells (7,16). In this study, using human PDAC tumor samples, we observed that MUC16 and MUC16-Cter showed significantly increased expression in liver metastasis than primary pancreatic tumors. Further, we have observed mechanistically that MUC16 induces/promotes tumorigenic and metastatic potential and vascular endothelial cell communication. We also studied the role of MUC16 in colonization in liver mimicking environment and MUC16 mediated mechanism for the metastasis of PC.

MUC16 on the cell surface interacts with mesothelin and galectin-3, significantly increasing PDAC cell motility and invasion. (7,39–41). MUC16 interaction with endothelial cells may

facilitate the tumor cell metastatic process. Vascular endothelial cells (ECs) have been associated with the modulation of cancer cells, subsequently enhancing their invasive and migratory ability (42). As cancer progresses, the inflammatory cytokines produced by cancer cells can stimulate the expression of E-selectin on ECs and enable the adhesion of cancer cells to the endothelium (43). E-selectin (CD62E), L-selectin (CD62L), and p-selectin (CD62P) have been associated with tethering and rolling of cancer cells on ECs (44). In addition, p-selectin and platelet aggregates facilitate the platelet-cancer cell interactions. This, in turn, leads platelets to protect the cancer cells from the innate immune system (45). Our observations significantly decreased human vascular endothelial cell binding and p-selectin binding in MUC16 manipulated PC cell models. These endothelial and p-selectin studies suggest that MUC16 expressing tumor cells promote the initial binding with endothelial cells. Subsequently, it may bind with platelets in circulation during the cascade of metastatic spread of PC cells.

The next goal was to analyze how MUC16 helps the tumor cells survive and colonize in a distant metastatic organ like the liver in pancreatic cancer. MUC16 knockdown cells decrease the survival and colonization in the anchorage-independent and liver mimicking *ex vivo* environment. Together, these results strongly prove the concept that MUC16 plays a critical role during metastatic liver colonization of PC cells.

Based on global RNA-seq data, MUC16 mediated metastatic genes, including NRP2 and cell adhesion molecules PCDHB12 and DSC3 in knockout and overexpression models, were identified to understand the mechanism of metastasis. Interestingly, NRP2 expression was decreased in MUC16 KD cells, whereas it was increased in MUC16-Cter overexpressed PC cells. NRP2 expression in tumor tissue is associated with tumor progression and metastasis (46). High expression of NRP2 can be seen on the surface of cancer cells from pancreatic neuroendocrine tumors (47) and pancreatic ductal adenocarcinomas (18). However, the molecular mechanisms through which NRP2 promotes tumor metastasis in pancreatic cancer remain unknown. The phosphorylation of JAK2 and STAT1 alteration was observed in MUC16 manipulated models along with NRP2 expression. MUC16-mediated JAK2/STAT1 pathway is involved in the regulation of NRP2 in pancreatic cancer cells. Moreover, NRP2 silenced PC cells showed decreased vascular endothelial, p-selectin binding, and migratory potential; this indicates that MUC16 mediated NRP2 expression induces metastasis in pancreatic cancer cells. Furthermore, MUC16-mediated enrichment of genes related to cell adhesion pathways suggests that MUC16 induces the heterotypic cell interaction for the metastasis of pancreatic cancer cells. Based on our data, MUC16 expression is directly associated with the expression of EMT markers in PC cells, suggesting that MUC16 induces the epithelial to mesenchymal transition and contributes to the metastatic behavior of PC cells.

Overall, this study demonstrates that MUC16 expressing tumor cells contribute to pancreatic cancer metastasis cascade. Together, our study provides the molecular mechanisms by which MUC16, particularly its carboxyl-terminal domain (MUC16-Cter), facilitates metastasis in pancreatic cancer. MUC16 promotes NRP2 expression through activation of JAK2/STAT1 signaling, which upholds tumor aggressiveness and liver metastasis in PDAC. Similarly, an in vivo hemi-spleen injected mouse model revealed that MUC16 promotes PDAC liver

metastasis. MUC16 mediated upregulation of cell adhesion molecules helps tumor cells bind to vascular endothelium during intravasation and interactions with platelets in circulation to protect the immune system, thereby helping tumor cells survive and recolonize in the liver metastasis. Therefore, targeting MUC16 might be an ideal therapeutic strategy for inhibiting tumorigenesis and metastasis of PDAC.

## Supplementary Material

Refer to Web version on PubMed Central for supplementary material.

## Acknowledgments

We thank Geoffrey A. Talmon for evaluating immunohistochemical staining. We thank Flow Cytometry Research Facility, University of Nebraska Medical Center, for assisting with flow cytometry. We thank Advanced Microscopy Core Facility at the University of Nebraska Medical Center for helping with confocal microscopy. We thank Genomics Core Facility at the University of Nebraska Medical Center for assisting with Next Generation Sequencing.

### Funding information

This work was supported by the National Institutes of Health P01 CA217798, R01 CA210637, R01 CA195586, R01 CA206444, R01 CA228524, U01 CA200466, and U01 CA210240.

## Data availability

The datasets used and/or analyzed during the current study are available from the corresponding author on reasonable request.

## References

1. Puckett Y, Garfield K. Pancreatic Cancer. StatPearls. Treasure Island (FL): StatPearls Publishing.Copyright © 2021, StatPearls Publishing LLC.; 2021.
2. Borazanci E, Sckolnik S, Amini A. Neo-adjuvant therapy for pancreatic cancer: hope for the future. Expert Rev Gastroenterol Hepatol 2019;13(6):579–89 doi 10.1080/17474124.2019.1607294. [PubMed: 30979348]
3. Wang X, Hu LP, Qin WT, Yang Q, Chen DY, Li Q, et al. Identification of a subset of immunosuppressive P2RX1-negative neutrophils in pancreatic cancer liver metastasis. Nat Commun 2021;12(1):174 doi 10.1038/s41467-020-20447-y. [PubMed: 33420030]
4. Young ED, Manley SJ, Beadnell TC, Shearin AE, Sasaki K, Zimmerman R, et al. Suppression of pancreatic cancer liver metastasis by secretion-deficient ITIH5. Br J Cancer 2021;124(1):166–75 doi 10.1038/s41416-020-01093-z. [PubMed: 33024269]
5. Haridas D, Ponnusamy MP, Chugh S, Lakshmanan I, Seshacharyulu P, Batra SK. MUC16: molecular analysis and its functional implications in benign and malignant conditions. Faseb j 2014;28(10):4183–99 doi 10.1096/fj.14-257352. [PubMed: 25002120]
6. Haridas D, Chakraborty S, Ponnusamy MP, Lakshmanan I, Rachagani S, Cruz E, et al. Pathobiological implications of MUC16 expression in pancreatic cancer. PLoS One 2011;6(10):e26839 doi 10.1371/journal.pone.0026839. [PubMed: 22066010]
7. Muniyan S, Haridas D, Chugh S, Rachagani S, Lakshmanan I, Gupta S, et al. MUC16 contributes to the metastasis of pancreatic ductal adenocarcinoma through focal adhesion mediated signaling mechanism. Genes Cancer 2016;7(3–4):110–24 doi 10.18632/genesandcancer.104. [PubMed: 27382435]
8. Felder M, Kapur A, Gonzalez-Bosquet J, Horibata S, Heintz J, Albrecht R, et al. MUC16 (CA125): tumor biomarker to cancer therapy, a work in progress. Mol Cancer 2014;13:129 doi 10.1186/1476-4598-13-129. [PubMed: 24886523]

9. Clarke CH, Yip C, Badgwell D, Fung ET, Coombes KR, Zhang Z, et al. Proteomic biomarkers apolipoprotein A1, truncated transthyretin and connective tissue activating protein III enhance the sensitivity of CA125 for detecting early stage epithelial ovarian cancer. Gynecol Oncol 2011;122(3):548–53 doi 10.1016/j.ygyno.2011.06.002. [PubMed: 21708402]
10. Shen H, Guo M, Wang L, Cui X. MUC16 facilitates cervical cancer progression via JAK2/STAT3 phosphorylation-mediated cyclooxygenase-2 expression. Genes Genomics 2020;42(2):127–33 doi 10.1007/s13258-019-00885-9. [PubMed: 31736008]
11. Lakshmanan I, Ponnusamy MP, Das S, Chakraborty S, Haridas D, Mukhopadhyay P, et al. MUC16 induced rapid G2/M transition via interactions with JAK2 for increased proliferation and anti-apoptosis in breast cancer cells. Oncogene 2012;31(7):805–17 doi 10.1038/onc.2011.297. [PubMed: 21785467]
12. Lakshmanan I, Salfity S, Seshacharyulu P, Rachagani S, Thomas A, Das S, et al. MUC16 Regulates TSPYL5 for Lung Cancer Cell Growth and Chemoresistance by Suppressing p53. Clin Cancer Res 2017;23(14):3906–17 doi 10.1158/1078-0432.Ccr-16-2530. [PubMed: 28196872]
13. Streppel MM, Vincent A, Mukherjee R, Campbell NR, Chen SH, Konstantopoulos K, et al. Mucin 16 (cancer antigen 125) expression in human tissues and cell lines and correlation with clinical outcome in adenocarcinomas of the pancreas, esophagus, stomach, and colon. Hum Pathol 2012;43(10):1755–63 doi 10.1016/j.humpath.2012.01.005. [PubMed: 22542127]
14. Liang C, Qin Y, Zhang B, Ji S, Shi S, Xu W, et al. Oncogenic KRAS Targets MUC16/CA125 in Pancreatic Ductal Adenocarcinoma. Mol Cancer Res 2017;15(2):201–12 doi 10.1158/1541-7786.Mcr-16-0296. [PubMed: 28108627]
15. Das S, Majhi PD, Al-Mugotir MH, Rachagani S, Sorgen P, Batra SK. Membrane proximal ectodomain cleavage of MUC16 occurs in the acidifying Golgi/post-Golgi compartments. Sci Rep 2015;5:9759 doi 10.1038/srep09759. [PubMed: 26044153]
16. Das S, Rachagani S, Torres-Gonzalez MP, Lakshmanan I, Majhi PD, Smith LM, et al. Carboxyl-terminal domain of MUC16 imparts tumorigenic and metastatic functions through nuclear translocation of JAK2 to pancreatic cancer cells. Oncotarget 2015;6(8):5772–87 doi 10.18632/oncotarget.3308. [PubMed: 25691062]
17. Borchardt H, Schulz A, Datta K, Muders MH, Aigner A. Silencing of Neuropilins and GIPC1 in pancreatic ductal adenocarcinoma exerts multiple cellular and molecular antitumor effects. Sci Rep 2019;9(1):15471 doi 10.1038/s41598-019-51881-8. [PubMed: 31664117]
18. Dallas NA, Gray MJ, Xia L, Fan F, van Buren G 2nd, Gaur P, et al. Neuropilin-2-mediated tumor growth and angiogenesis in pancreatic adenocarcinoma. Clin Cancer Res 2008;14(24):8052–60 doi 10.1158/1078-0432.Ccr-08-1520. [PubMed: 19088020]
19. Fukahi K, Fukasawa M, Neufeld G, Itakura J, Korc M. Aberrant expression of neuropilin-1 and −2 in human pancreatic cancer cells. Clin Cancer Res 2004;10(2):581–90 doi 10.1158/1078-0432.ccr-0930-03. [PubMed: 14760080]
20. Muders MH. Neuropilin and neuropilin associated molecules as new molecular targets in pancreatic adenocarcinoma. Anticancer Agents Med Chem 2011;11(5):442–7 doi 10.2174/187152011795677481. [PubMed: 21492075]
21. Gray MJ, Van Buren G, Dallas NA, Xia L, Wang X, Yang AD, et al. Therapeutic targeting of neuropilin-2 on colorectal carcinoma cells implanted in the murine liver. J Natl Cancer Inst 2008;100(2):109–20 doi 10.1093/jnci/djm279. [PubMed: 18182619]
22. Handa A, Tokunaga T, Tsuchida T, Lee YH, Kijima H, Yamazaki H, et al. Neuropilin-2 expression affects the increased vascularization and is a prognostic factor in osteosarcoma. Int J Oncol 2000;17(2):291–5 doi 10.3892/ijo.17.2.291. [PubMed: 10891538]
23. Polavaram NS, Dutta S, Islam R, Bag AK, Roy S, Poitz D, et al. Tumor- and osteoclast-derived NRP2 in prostate cancer bone metastases. Bone Res 2021;9(1):24 doi 10.1038/s41413-021-00136-2. [PubMed: 33990538]
24. Yasuoka H, Kodama R, Tsujimoto M, Yoshidome K, Akamatsu H, Nakahara M, et al. Neuropilin-2 expression in breast cancer: correlation with lymph node metastasis, poor prognosis, and regulation of CXCR4 expression. BMC Cancer 2009;9:220 doi 10.1186/1471-2407-9-220. [PubMed: 19580679]

25. Cao Y, Hoeppner LH, Bach S, E G, Guo Y, Wang E, et al. Neuropilin-2 promotes extravasation and metastasis by interacting with endothelial α5 integrin. Cancer Res 2013;73(14):4579–90 doi 10.1158/0008-5472.Can-13-0529. [PubMed: 23689123]
26. Kaushik G, Ponnusamy MP, Batra SK. Concise Review: Current Status of Three-Dimensional Organoids as Preclinical Models. STEM CELLS 2018;36(9):1329–40 doi 10.1002/stem.2852. [PubMed: 29770526]
27. Li G, Kim YJ, Mantel C, Broxmeyer HE. P-selectin enhances generation of CD14+CD16+ dendritic-like cells and inhibits macrophage maturation from human peripheral blood monocytes. J Immunol 2003;171(2):669–77 doi 10.4049/jimmunol.171.2.669. [PubMed: 12847232]
28. Nimmakayala RK, Leon F, Rachagani S, Rauth S, Nallasamy P, Marimuthu S, et al. Metabolic programming of distinct cancer stem cells promotes metastasis of pancreatic ductal adenocarcinoma. Oncogene 2021;40(1):215–31 doi 10.1038/s41388-020-01518-2. [PubMed: 33110235]
29. Soares KC, Foley K, Olino K, Leubner A, Mayo SC, Jain A, et al. A preclinical murine model of hepatic metastases. J Vis Exp 2014(91):51677 doi 10.3791/51677. [PubMed: 25285458]
30. Mallya K, Gautam SK, Aithal A, Batra SK, Jain M. Modeling pancreatic cancer in mice for experimental therapeutics. Biochim Biophys Acta Rev Cancer 2021;1876(1):188554 doi 10.1016/j.bbcan.2021.188554. [PubMed: 33945847]
31. Ramamoorthy P, Thomas SM, Kaushik G, Subramaniam D, Chastain KM, Dhar A, et al. Metastatic Tumor-in-a-Dish, a Novel Multicellular Organoid to Study Lung Colonization and Predict Therapeutic Response. Cancer Res 2019;79(7):1681–95 doi 10.1158/0008-5472.Can-18-2602. [PubMed: 30674533]
32. Bendas G, Borsig L. Cancer cell adhesion and metastasis: selectins, integrins, and the inhibitory potential of heparins. Int J Cell Biol 2012;2012:676731 doi 10.1155/2012/676731. [PubMed: 22505933]
33. Garrido-Laguna I, Hidalgo M. Pancreatic cancer: from state-of-the-art treatments to promising novel therapies. Nat Rev Clin Oncol 2015;12(6):319–34 doi 10.1038/nrclinonc.2015.53. [PubMed: 25824606]
34. Yachida S, Iacobuzio-Donahue CA. The pathology and genetics of metastatic pancreatic cancer. Arch Pathol Lab Med 2009;133(3):413–22 doi 10.1043/1543-2165-133.3.413. [PubMed: 19260747]
35. Disibio G, French SW. Metastatic patterns of cancers: results from a large autopsy study. Arch Pathol Lab Med 2008;132(6):931–9 doi 10.1043/1543-2165(2008)132[931:Mpocrf]2.0.Co;2. [PubMed: 18517275]
36. Huang C, Li N, Li Z, Chang A, Chen Y, Zhao T, et al. Tumour-derived Interleukin 35 promotes pancreatic ductal adenocarcinoma cell extravasation and metastasis by inducing ICAM1 expression. Nat Commun 2017;8:14035 doi 10.1038/ncomms14035. [PubMed: 28102193]
37. Comamala M, Pinard M, Thériault C, Matte I, Albert A, Boivin M, et al. Downregulation of cell surface CA125/MUC16 induces epithelial-to-mesenchymal transition and restores EGFR signalling in NIH:OVCAR3 ovarian carcinoma cells. British journal of cancer 2011;104(6):989–99 doi 10.1038/bjc.2011.34. [PubMed: 21326240]
38. Giannakouros P, Comamala M, Matte I, Rancourt C, Piché A. MUC16 mucin (CA125) regulates the formation of multicellular aggregates by altering β-catenin signaling. American journal of cancer research 2014;5(1):219–30. [PubMed: 25628932]
39. Einama T, Kamachi H, Nishihara H, Homma S, Kanno H, Takahashi K, et al. Coexpression of mesothelin and CA125 correlates with unfavorable patient outcome in pancreatic ductal adenocarcinoma. Pancreas 2011;40(8):1276–82 doi 10.1097/MPA.0b013e318221bed8. [PubMed: 21775916]
40. Shimizu A, Hirono S, Tani M, Kawai M, Okada K, Miyazawa M, et al. Coexpression of MUC16 and mesothelin is related to the invasion process in pancreatic ductal adenocarcinoma. Cancer Sci 2012;103(4):739–46 doi 10.1111/j.1349-7006.2012.02214.x. [PubMed: 22320398]
41. Chen SH, Hung WC, Wang P, Paul C, Konstantopoulos K. Mesothelin binding to CA125/MUC16 promotes pancreatic cancer cell motility and invasion via MMP-7 activation. Sci Rep 2013;3:1870 doi 10.1038/srep01870. [PubMed: 23694968]

42. Shenoy AK, Lu J. Cancer cells remodel themselves and vasculature to overcome the endothelial barrier. Cancer Lett 2016;380(2):534–44 doi 10.1016/j.canlet.2014.10.031. [PubMed: 25449784]

43. Reymond N, d'Água BB, Ridley AJ. Crossing the endothelial barrier during metastasis. Nat Rev Cancer 2013;13(12):858–70 doi 10.1038/nrc3628. [PubMed: 24263189]

44. Barthel SR, Gavino JD, Descheny L, Dimitroff CJ. Targeting selectins and selectin ligands in inflammation and cancer. Expert Opin Ther Targets 2007;11(11):1473–91 doi 10.1517/14728222.11.11.1473. [PubMed: 18028011]

45. Läubli H, Borsig L. Selectins promote tumor metastasis. Semin Cancer Biol 2010;20(3):169–77 doi 10.1016/j.semcancer.2010.04.005. [PubMed: 20452433]

46. Yasuoka H, Kodama R, Hirokawa M, Takamura Y, Miyauchi A, Inagaki M, et al. Neuropilin-2 expression in papillary thyroid carcinoma: correlation with VEGF-D expression, lymph node metastasis, and VEGF-D-induced aggressive cancer cell phenotype. J Clin Endocrinol Metab 2011;96(11):E1857–61 doi 10.1210/jc.2011-1180. [PubMed: 21880798]

47. Cohen T, Herzog Y, Brodzky A, Greenson JK, Eldar S, Gluzman-Poltorak Z, et al. Neuropilin-2 is a novel marker expressed in pancreatic islet cells and endocrine pancreatic tumours. J Pathol 2002;198(1):77–82 doi 10.1002/path.1179. [PubMed: 12210066]

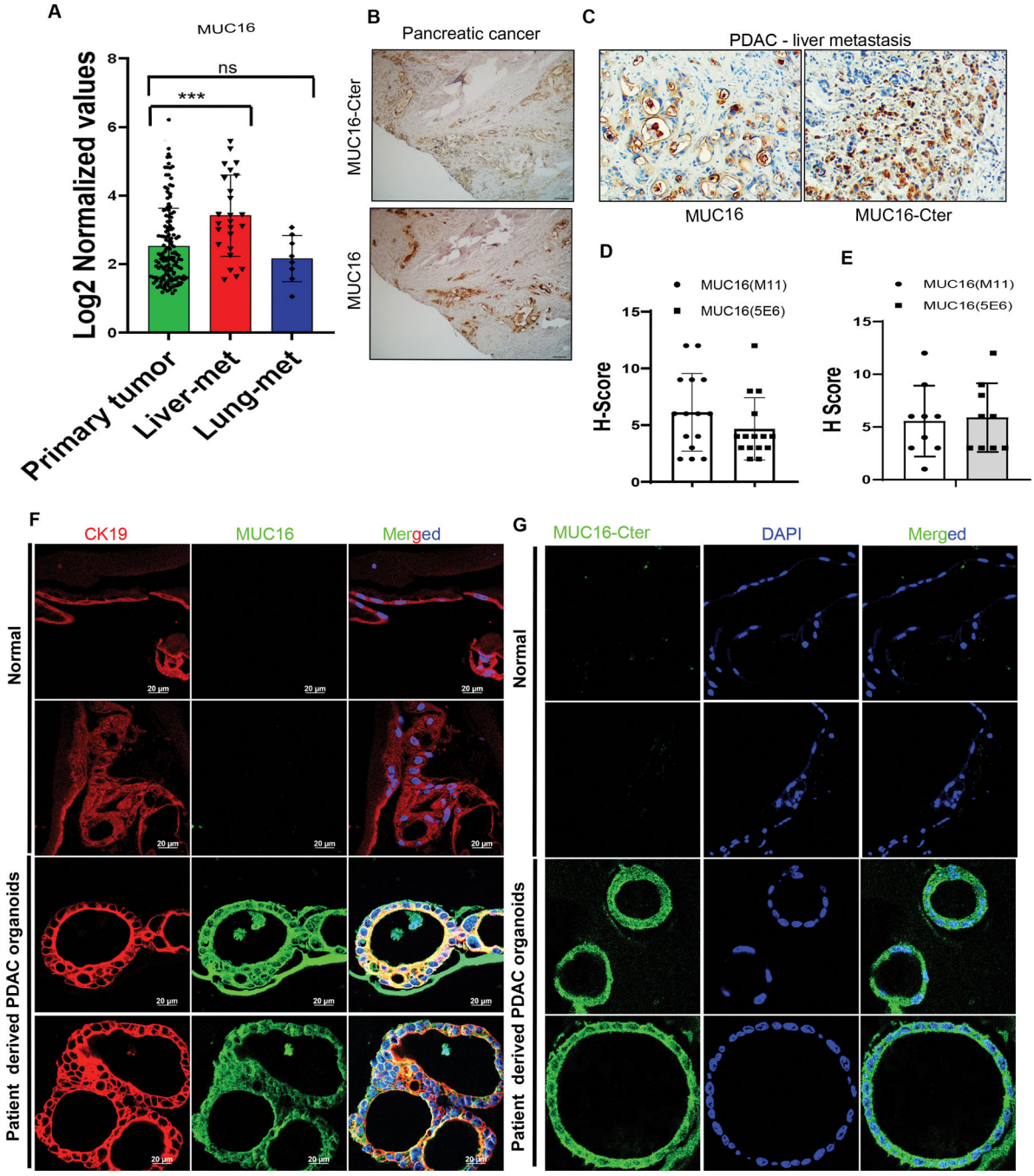


**Figure 1. Immunohistochemical staining of MUC16 and MUC16-Cter in human pancreatic cancer primary tumor, liver metastasis samples, and patient-derived PDAC organoids.**

A) Analysis of MUC16 expression profiles from the GEO database (GSE71729) in human PDAC primary tumor (n=145) liver metastasis (n = 25) and lung metastasis (n = 7). Data are mean ± SD. B) Immunohistochemically stained MUC16 and MUC16-Cter expression in human PDAC primary Whipple tumor tissues. C) Immunohistochemically stained MUC16 and MUC16-Cter expression in human PC liver-metastasis and lung-metastasis tissue microarrays (TMAs). D, E). The bar graph demonstrates the H-score of immunostaining of MUC16 and MUC16-Cter (scale bar, 100 μm). F, G) Immunofluorescence staining of CK19

(red) marker of ductal adenocarcinomas and MUC16 (green) and MUC16-Cter (green) in human PDAC derived organoid (n = 8) and normal tissues (n = 5) (scale bar, 20 μm).

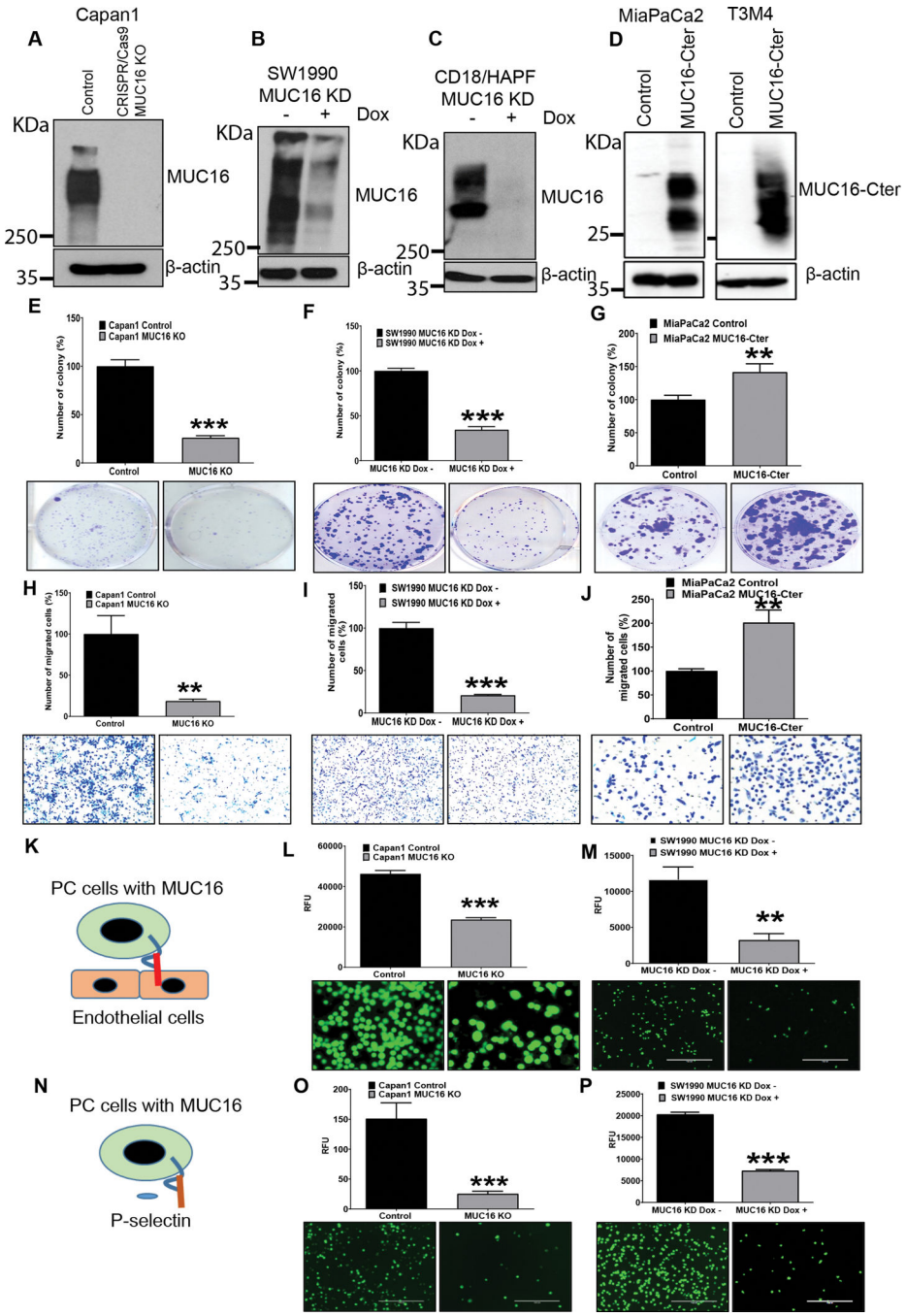


**Figure 2. MUC16 silencing decreases the *in vitro* tumorigenic, migratory potential, and endothelial/p-selectin binding in PC.**

A, B, C) MUC16 expression was determined in MUC16 silenced PC cells (Capan1 CRISPR/Cas9 based KO, SW1990 MUC16 KD and CD18/HPAF MUC16 KD cells) by immunoblot. D) MUC16-Cter expression in MUC16-Cter overexpressed MiaPaCa2 and T3M4 cells by immunoblot. E, F) *In vitro* tumorigenic capability significantly decreased in MUC16 knockout Capan1 cells and doxycycline-inducible SW1990 MUC16 KD cells with their respective control cells. G) MUC16-Cter overexpressed cells show significantly increased tumorigenic capability in MiaPaCa2 MUC16-Cter cells compared to the control

cells. Data represent ± standard deviation (p values are calculated by ‘ ‘Student’s t-test (***p<0.001, **p<0.01) (n=3). H, I) Migratory potential significantly reduced in Capan1 MUC16 KO, SW1990 MUC16 KD cells and their respective control cells. J) MiaPaCa2 MUC16-Cter cells show significantly increased migratory potential compared to the control cells. Data represent ± standard deviation (p values are calculated by ‘ ‘Student’s t-test (***p<0.001, **p<0.01) (n=3). K, L, M) Tumor cell - endothelial (HMEC1) binding study show Capan1 MUC16 KO and SW1990 MUC16 KD cells significantly decrease endothelial binding compared to the MUC16 expressing cells. N, O, P) Human p-selectin/CD62P immunoassay shows Capan1 MUC16 KO and SW1990 MUC16 KD cells significantly decreased compared to the control cells. Scale bar, 100 μm. Data represents ± standard deviation (p values are calculated by Student’s t-test (***p<0.001, **p<0.01) (n=3).

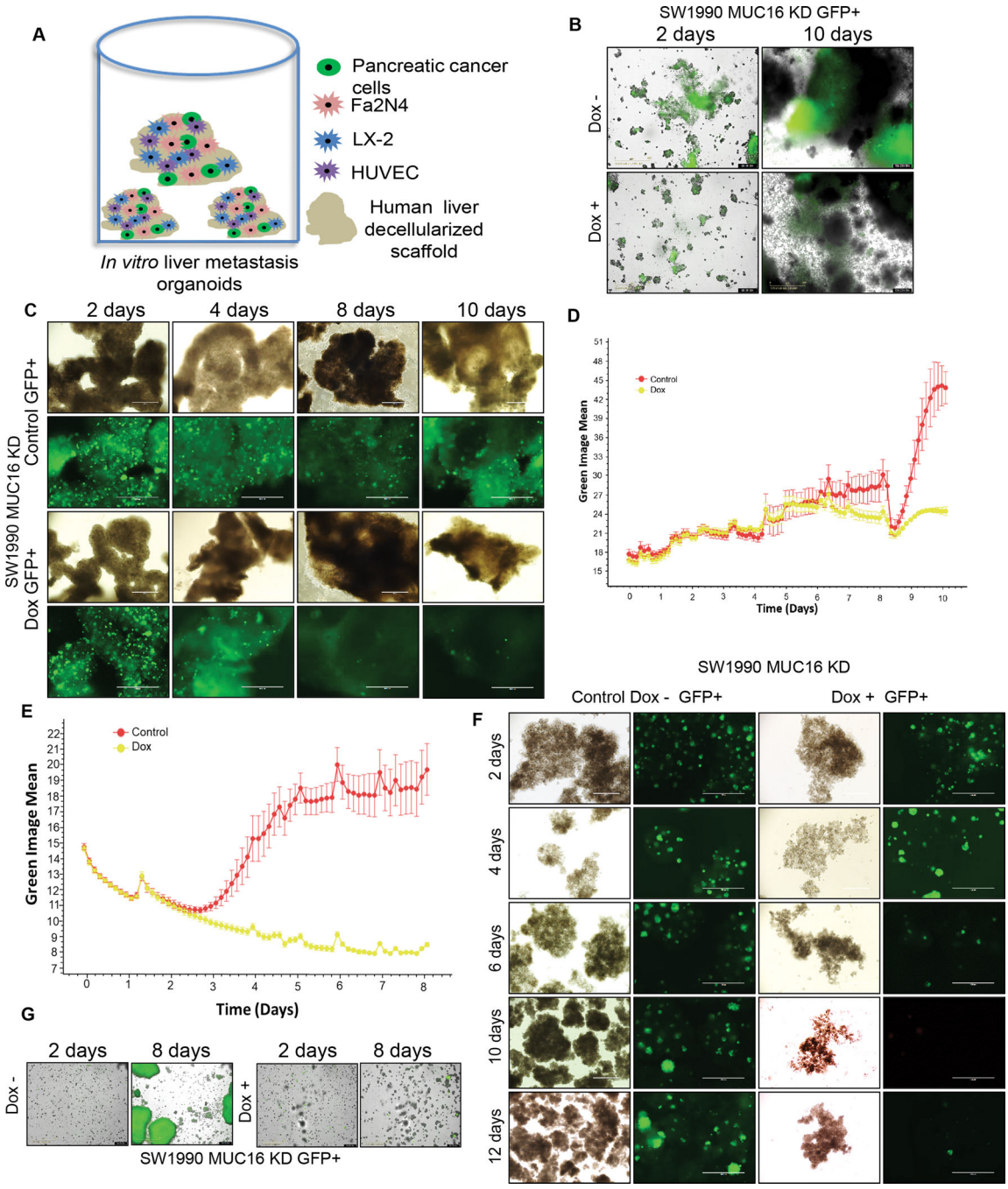


**Figure 3. MUC16 promotes cell survival and colonization potential *in vitro* liver metastasis model.**

A) Schematic illustration showing the strategy of *in vitro* liver metastatic model. For the liver-metastasis model, inducible MUC16 shRNA expressing PC (SW1990) cells were mixed with Fa2N4, LX-2, HUVEC cells, and human decellularized liver scaffold was mixed and grown in ultra-low attachment 96 well plates in DMEM-F12 with supplements. B, C) SW1990 MUC16 KD $GFP^{+}$ 3D culture was treated with or without doxycycline, and the green, the fluorescent image was captured at different times (2 to 10 days). Representative GFP images were generated from automated live-cell imaging, a bright field microscope,

and an immunofluorescence image of 3D culture. D) SW1990 MUC16 KD $GFP^+$ cells grown in *in vitro* settings impersonating liver metastasis model. The growth curve is generated based on the green fluorescent protein expression in 3D culture. E) MUC16 expressing pancreatic cancer SW1990 cells clonogenic anchorage-independent cell growth curve. F, G) Light microscopy images of the sphere and corresponding green fluorescence images and GFP images from Incucyte were taken at different time points (2 to 12 days).

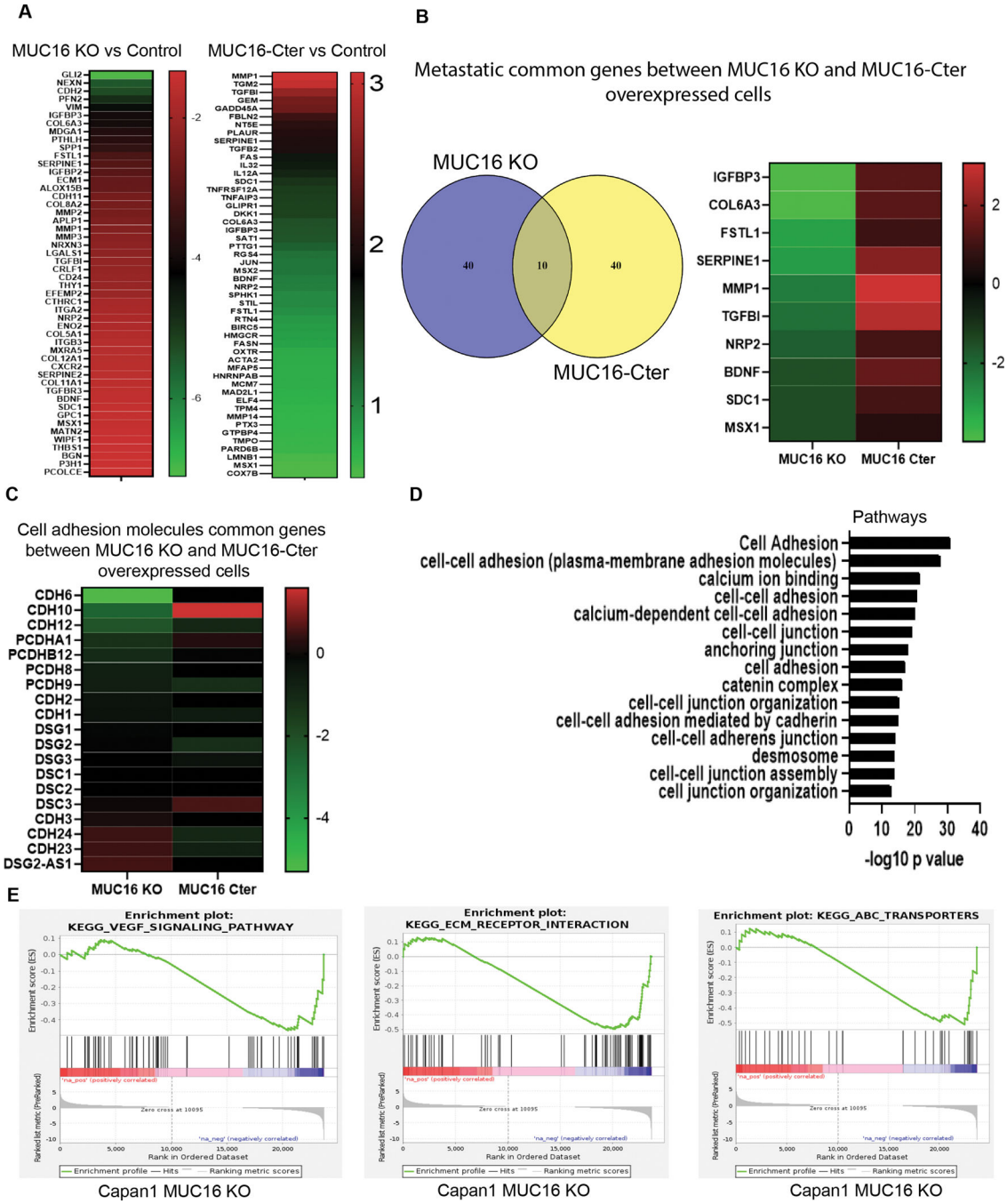


**Figure 4. Identifying the cell adhesion and metastatic genes expression in MUC16 Knockout and MUC16-Cter overexpressed cells from global RNA-seq**

A) Heat map shows the top 50 genes altered in MUC16 KO and MUC16-Cter overexpressed cells from our RNA-seq data. B) Venn diagram shows the common 10 genes identified between MUC16 KO and MUC16 overexpressed cells. The heat map shows commonly altered genes (IGFBP2, COL6A3, FSTL1, SERPINE1, MMP1, TGFBI, NRP2, BDNF, SDC1, and MSX1). C) Heat map shows top 19 altered common genes associated with cell adhesion molecules. D) Pathway enrichment analysis from MUC16 KO cells shows cell

adhesion and cell-cell junction-associated pathways. Based on – log10 p-value. E) VEGF, ECM, and ABC pathway enrichment plots generated from MUC16 KO Capan1 PC cells.

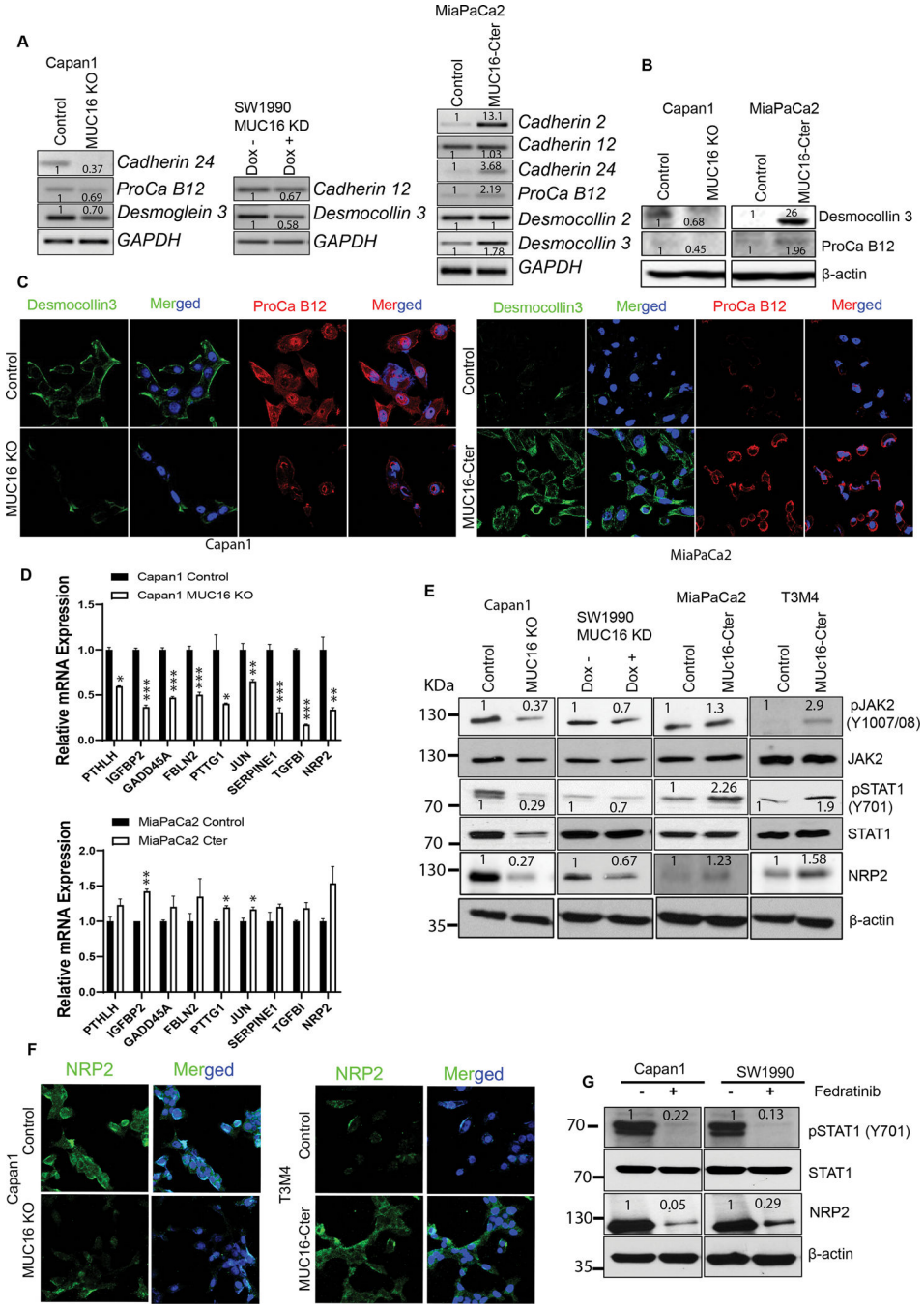


**Figure 5. MUC16 regulation of cell adhesion-promoting molecules and metastatic gene NRP2 regulation through activation of JAK2/STAT1 axis**

A) PCR analysis shows mRNA expression of cell adhesion molecules in Capan1 MUC16 KO, SW1990 MUC16 KD, and MUC16-Cter overexpressed MiaPaCa2 cells with control cells. GAPDH was used as a loading control. B, C) Immunoblot and immunofluorescent staining of cell adhesion molecules, Desmocollin 3 (green) and Protocadherin B12 (red) expression in MUC16 KO and MUC16-Cter overexpressed PC cells with respective control cells. Immunofluorescence images were taken under the confocal microscope; scale bar, 50 μm. D) QRT-PCR validation of 10 common genes in Capan1 MUC16 KO and MiaPaCa2

MUC16-Cter overexpressed cells. Data represent ± standard deviation (Student's t-test calculates p values (***p<0.001, **p<0.01, *p<0.05) (n=3). E) Immunoblot analysis shows the phospho-JAK2 (Y1007/1008), total JAK2, phospho-STAT1 (Y701), total STAT1 and NRP2 expression in Capan1 MUC16 KO, SW1990 MUC16 KD, MiaPaCa2 MUC16-Cter, and T3M4 MUC16-Cter overexpressed cells. β-actin was used as a loading control. F) Immunofluorescence analysis was performed to show the NRP2 expression in MUC16 KO and MUC16-Cter overexpressed PC cells. Images were obtained from a confocal microscope; scale bar, 50 μm. G) Effect of silencing the JAK2 activation using JAK2 inhibitor (Fedratinib) in Capan1 and SW1990 cells. Immunoblot analysis shows the phospho-STAT1 (Y701), total STAT1, and NRP2 expression in Capan1 and SW1990 cells. β-actin was used as a loading control. Western blots were quantified by densitometric analysis.

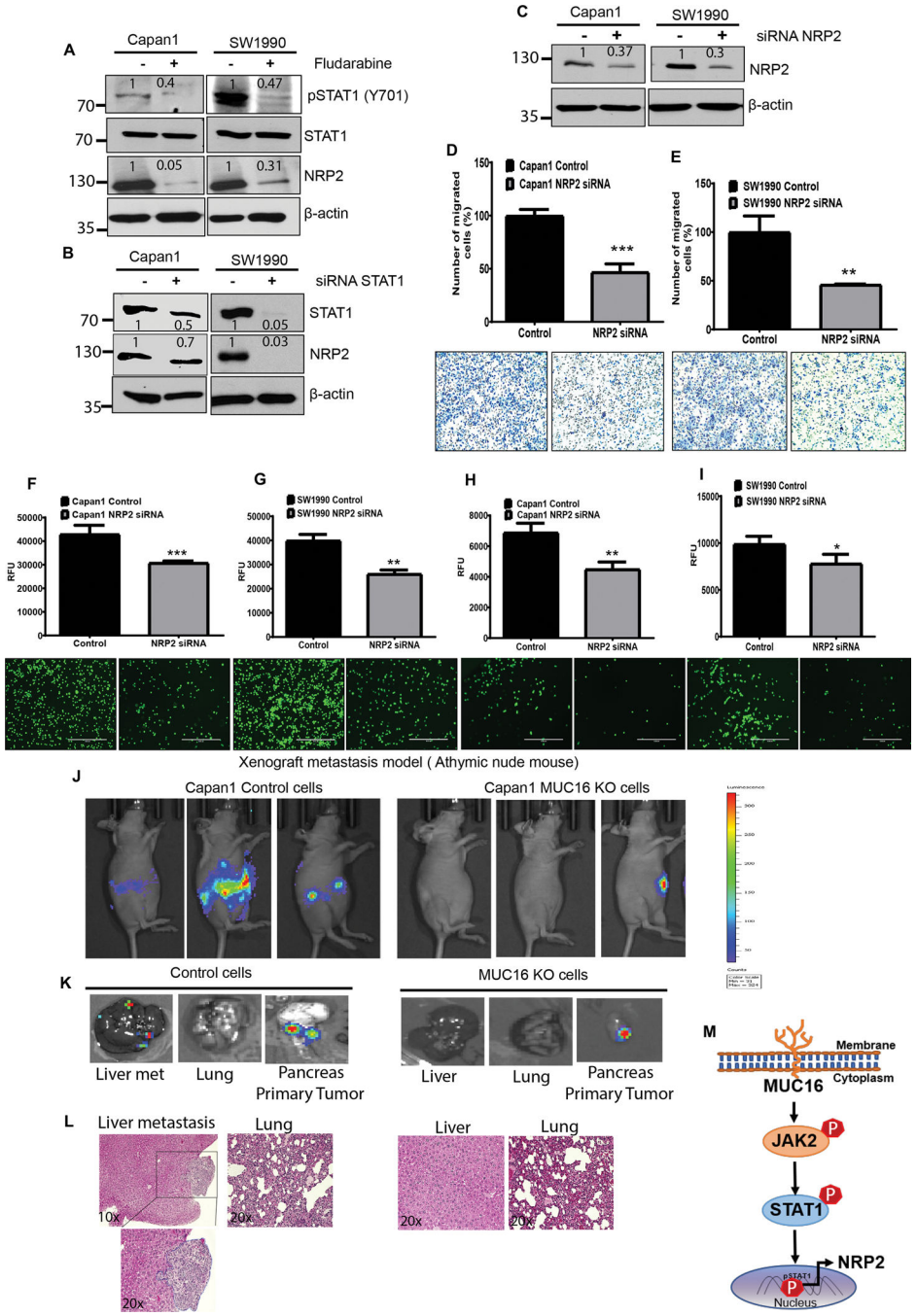


**Figure 6. Loss of NRP2 decreases the endothelial, p-selectin binding, and migratory potential in PC cells**

A, B) STAT1 inhibitor (Fludarabine) or Small interfering RNA (siRNA) silencing of STAT1 in Capan1 and SW1990 cells. Immunoblot analysis shows the effect of STAT1 silencing on NRP2 expression. β-actin was used as a loading control. C) NRP2 knockdown determined in NRP2 siRNA expressed in PC (Capan1 and SW1990) cells by western blot. D, E) Migratory potential decreased in NRP2 silenced in Capan1 and SW1990 cells compared to control cells. Data represent ± standard deviation (p values are calculated by ‘ ‘Student’s t-test (***p<0.001, **p<0.01) (n=3). F-I) Effect of NRP2 silencing in Capan1

and SW1990 cells show significantly decreased endothelial and p-selectin binding compared to the control cells. Representative images were taken under the fluorescence microscope Scale bar, 100 μm. Data represent ± SD (p values are calculated by S' 'Student' 's t-test (***p<0.001, **p<0.01, *p<0.05) (n=3). MUC16 expression increases metastasis in the hemi-spleen mouse model. J) *In vivo* tumor growth and metastasis were imaged using an IVIS imaging system after intraperitoneal injection (IP) of D-luciferin at 21 days in Athymic nude mice. K) Representative IVIS image of PADC liver metastasis, lung and injected site of the pancreas tumor. L) Representative eosin staining of control and MUC16 KO cells injected hemi-spleen in athymic nude mice shown PDAC liver metastasis. M) Schematic representation demonstrates that MUC16 activates oncogenic signaling through pJAK2 (Y1007/1008) and pSTAT1 (Y701). Phosphorylation and nuclear localization of STAT1 lead to the upregulation of NRP2 and promotes PC metastasis. Besides, MUC16 correspondingly promotes cell adhesion molecules during PC liver metastasis. Western blots were quantified by densitometric analysis.